Differential degradation of RNA species by autophagy related pathways in plants

Hickl[a1], D., Drews[b,c*1], F., Girke[a], C., Zimmer[d], D., Mühlhaus[d], T., Hauth[e], J., Nordström[f], K., Trentmann[a], O., Neuhaus[a], H.E., Fehlmann[g], T., Keller[g,h], A., Simon[b], M., and Möhlmann, T.[a*]

[a] Department of Biology, Plant Physiology, University of Kaiserslautern, Kaiserslautern, Germany
[b] Department of Biology, Molecular Cell Biology, Wuppertal University, Wuppertal, Germany
[c] Molecular Cell Dynamics, Saarland University, Saarbrücken, Germany
[d] Department of Biology, Computational Systems Biology, University of Kaiserslautern, Kaiserslautern, Germany
[e] Fraunhofer Institute for Industrial Mathematics ITWM, Kaiserslautern, Germany
[f] Department of Genetics, Saarland University, Saarbrücken, Germany
[g] Chair for Clinical Bioinformatics, Saarland University, Saarbrücken, Germany
[h] Stanford, School of Medicine, Ca, USA

[1] authors contributed equally

*Corresponding author
Dr. Torsten Möhlmann
Universität Kaiserslautern, Pflanzenphysiologie
Postfach 3049, D-67653 Kaiserslautern, Germany
moehlmann@biologie.uni-kl.de

Keywords: Vacuole, RNase, ATG5, RNA sequencing, Barley, Arabidopsis

Word count: 7351

Abstract

An important function of the plant vacuole is the recycling of the delivered proteins and RNA by autophagy. We provide the first plant vacuolar small RNome by isolation of intact vacuoles from Barley and Arabidopsis, subsequent RNA purification and Next Generation Sequencing. In these vacuolar sRNomes, all types of cellular RNAs were found including those of chloroplast origin, suggesting a bulk-type of RNA transfer to, and breakdown in vacuoles. ATG5 is a major representative of autophagy genes and the vacuolar RNA composition in corresponding knockout plants differed clearly from controls as most chloroplast derived RNA species were missing. Moreover, the read length distribution of RNAs found in ATG5 mutants differed to control samples, indicating altered RNA processing. In contrast, vacuoloar RNA length and composition of plants lacking the vacuolar RNase2 (*rns2-2*), involved in cellular RNA homeostasis, showed minor alterations, only. Our data therefore suggests that mainly autophagy components are responsible for selective transport and targeting of different RNA species into the vacuole for degradation. In addition to short RNA fragments of longer RNAs, mature miRNAs were detected in all vacuolar preparations, however in ATG5 mutants at much lower frequency. Read length analysis indicates that vacuolar miRNAs are not degradet suggesting an additional RNA targeting mechanism and a potential new role biological for vacuolar miRNAs.

.

Introduction

Vacuoles fulfil many functions in plant metabolism. They are responsible for the maintenance of turgor pressure and they are storage compartments for sugars, organic acids, amino acids and ions (Trentmann et al., 2014; Hedrich et al., 2015). Furthermore, vacuoles are also a site for breakdown of cellular macromolecules. The role in RNA degradation was assigned to vacuoles based on the observation of 80% of total cellular RNase activity in this compartment (Boller and Kende, 1979). This was further supported by others (Abel & Glund 1986, 1987) and later, evidence for the presence of RNA-oligonucleotides in isolated vacuoles from cultured tomato cells was presented (Abel et al., 1990). Bariola et al., (1999) identified RNS2, a member of the T2 RNase family from Arabidopsis as vacuolar RNase and Hillwig et al. (2011) describe this enzyme as necessary for ribosomal RNA decay and found that corresponding knockout mutants showed a constitutive autophagy. In the same year, with ENT1 (equilibrative nucleoside transporter 1) a vacuolar transport protein was identified, responsible for the export of RNA breakdown products in form of nucleosides (Bernard et al., 2011).

Based on these findings it is clear that plant vacuoles are important sites for cellular RNA catabolism. However, the types of RNA delivered to the vacuole and the identity of catabolic enzymes are so far unknown.

Macroautophagy (termed autophagy in the remaining of the manuscript) is a process that delivers unwanted cellular material and organelles to the vacuole for degradation (Michaeli et al., 2014). In yeast, autophagy was identified as mechanism involved in bulk RNA degradation induced by starvation, pointing to the importance of rRNA turnover e.g. as nitrogen source under stress conditions (Huang et al., 2014). In line with this, Arabidopsis plants lacking the vacuolar RNase2 (RNS2) show constitutive autophagy,

even under normal growth conditions, emphasizing the role of RNA recycling for plant homeostasis (Hillwig et al., 2011, Bassham and MacIntosh, 2017).

Bassham and MacIntosh (2017) state in the Abstract of their review on autophagy mediated degradation of ribosomes: ”Ribosomes are essential molecular machines that require a large cellular investment, yet the mechanisms of their turnover are not well understood in any eukaryotic organism. Recent advances in Arabidopsis suggest that plants utilize selective mechanisms to transport rRNA or ribosomes to the vacuole, where rRNA is degraded and the breakdown products recycled to maintain cellular homeostasis”.

To address this topic we developed a protocol, allowing quantitative and qualitative analysis of the vacuolar RNome. Therefore, we have isolated vacuoles from Arabidopsis and towards a general validity in addition from Barley (*Hordeum vulgare*) as a monocot species with agronomical significance. In a novel approach we sequenced the RNome of this organelle to obtain information on the type of RNA at single sequence resolution. Furthermore, we included mutants lacking components of the autophagy process (ATG5) and the RNA catabolism (RNS2) in our analysis.

Results

In our project we aimed for the identification of RNA species inside plant vacuoles at single sequence resolution. We chose Barley (*Hordeum vulgare*) as an agronomically important monocot plant and Arabidopsis as a general plant model. Although, detailed protocols for the isolation of highly pure vacuoles for both species exist, we had to develop a strategy for the investigation of vacuolar RNA composition. Thus, subsequent to vacuole isolation, RNA was extracted, converted into Illumina compatible libraries and subjected to deep sequencing followed by bioinformatic analysis.

Barley vacuoles contain short RNA fragments mainly belonging to chloroplast RNAs

For vacuole isolation, primary leaves from 8-9 day old Barley (*Hordeum vulgare* type "Barke") plants were harvested at the beginning of the light period, following available protocols (Rentsch and Martinoia, 1991, see Methods). Purified vacuoles were microscopically inspected and found to be intact and free of contaminating protoplasts (Figure 1 A). To obtain first indications for the presence of RNA species inside vacuoles, these were incubated with the RNA specific SYTO® RNASelect™ Green Fluorescent cell stain. Using this dye a clear green fluorescence from the vacuolar lumen was observed (Figure 1B-D). Since the presence of ribosomal RNA (rRNA) in plant vacuoles was shown before (Floyd et al., 2015; Hillwig et al., 2011), we checked for the presence of rRNA species in our isolated barley vacuoles. For this, RNA extracted from isolated vacuoles was subjected to northern blot and hybridized with 5S rRNA and 18S rRNA probes. In both cases, small fragments (below 120 nt) were labelled. Smallest fragments were app. 30 nt for the 5S probe and 50 nt for the 18S probe (Figure 1 E). To allow for a better and quantitative estimation of the RNA size distribution, total vacuolar RNA was

run on an Agilent small RNA Chip (BioAnalyzer 2100, Agilent Technologies, Santa Clara, USA). The majority of RNA corresponded to a fragment size of 25 to 200 nt (Figure 1F). Intact ribosomal RNA was absent from the sample, supporting a high purity and low contamination of the isolated vacuoles. Following our aim for a description of the vacuolar RNome at sequence level resolution, a RNA library was constructed and subsequently Illumina sequencing was performed on a HiSeq 2500 (Illumina, San Diego, USA), and obtained reads were trimmed removing reads <15 nt and mapped to the available Barley annotated genome (The International Barley Genome Sequencing Consortium, 2012). The distribution of the top 12 of all mapped reads to gene loci is shown in the pie chart (Figure 1G). Most prominent were reads mapping to the chloroplast 16S rRNA gene (gene id = HORVU2Hr1G062290) with 52% of top 12 reads. Three loci encode cell wall associated hydrolases (HORVU2Hr1G062280, HORVU7Hr1G064930, HORVU6Hr1G046740; total of 31% of top 12 reads). At positions 4-6 and 8-12 in our ranking we find photosynthesis associated nuclear genes (phang) rbscL, pSBA, pSBD, and Cp43 (Figure 1G, Supplemental Table S1 (htseq count_barley)).

Arabidopsis vacuoles contain short RNA fragments belonging to rRNA, tRNA and mRNA derived from cytosol and chloroplasts

In a second step we aimed to decipher the vacuolar RNome from Arabidopsis. For this we applied two slightly differing protocols for the isolation of vacuoles. A first protocol requires small leaves from plants that have not been singularized after sowing. (Robert et al., 2007; referred to as R-type vacuoles). The alternative method uses rosette leaves from individually grown Arabidopsis plants (Burla et al., 2013, referred to as B-type vacuoles). Based on marker enzyme activities, extravacuolar contaminations were investigated. Uridine diphosphate glucose pyrophosphorylase activity (UGPase, representing cytosol

and intact protoplasts) was 3.44%± 0.71 for R-type and 10.8% ± 3.55 for B-type vacuoles, compared to intact protoplasts. Contamination of purified vacuoles by chloroplasts was detected by Glycerine aldehyd-3-phosphate dehydrogenase activity and was below the detection level for R-type vacuoles and 3.54%± 0.78 for B-type vacuoles compared to intact protoplasts (Figure 2A).

To check for the presence of RNA within the vacuoles, the preparations were incubated with the RNA specific dye SYTO® RNASelect™ and the lipophilic dye FM4-64. The staining reveals presence of RNA inside B-type vacuoles (Figure 2B), whereas no fluorescence signal was detected in R-type vacuoles. Treatment of intact B-type vacuoles with RNase A prior to staining did not diminish the SYTO RNASelect signal from the vacuolar interior (Figure 2B) indicating protection of RNA against external RNase by the tonoplast.

For a quantitative readout of probable RNA contaminations R-type vacuoles were treated with different concentrations of RNase A and RNase A plus proteinase K. Latter controls will inactivate residual RNase A activity that could interfere with RNA isolation from vacuoles. Isolated vacuolar RNA was then end-labelled using P^{32}-CTP and separated on RNA PAGE. In all lanes most intense labelling was observed at a size of 29 to 48 nt. No obvious difference between treated and untreated samples was observed supporting our previous investigation, that RNA was protected from external RNase by the tonoplast (Figure 2C).

For B-type vacuoles we used RNA chip analysis to detect effects of RNAse A treatment on the size distribution of isolated vacuolar RNA. Whereas a few larger RNAs could be removed by RNase A treatment (Figure 2D), the smaller fraction of RNA was fully protected against degradation (Figure 2E). As a positive control for the functionality of

the RNase A treatment, lysed vacuoles were treated with this enzyme and as expected, all RNA was completely degraded (Figure 2F).

Comparing RNA contents from the two different vacuolar preparations

In a next step we subjected isolated RNA from R-type and B-type vacuoles to small RNA library preparation. RNA was isolated from at least three individual preparations of vacuoles. To obtain a higher read number and thus a better coverage during the mapping procedure, Illumina sequencing was performed on a HiSeq 2500 (Illumina, San Diego, USA), with 6M and 9M sequences obtained per library, see methods for details of the procedure. Obtained sequences were trimmed, removing sequences <15 nt and mapped to the Arabidopsis genome (Araport11) with corrections given in Supplemental file S4. Results from one sequencing run for each vacuole type are shown. In R-type vacuoles, the majority of sequencing reads were mapped to cytosolic rRNA loci (84.14%, Figure 2G). With 63% of all reads, the 25S species of cytosolic rRNA is the dominating one. Chloroplast rRNAs, tRNAs and mRNAs follow with 6.14%, 4.75% and 3.82%, respectively (Figure 2G). 0.71% of all reads are distributed among small RNA species as mi-RNA, sno-RNA, nc-RNA and sn-RNA (Figure 2G). Comparing these results with those from B-type vacuoles, the following observations can be made: First, cytosolic rRNA is also the dominant RNA species in B-type vacuoles, with 45.72% of all reads (Figure 2G). The reduction compared to R-type vacuoles is mainly due to reduced reads for 25S rRNA, dropping from 63% to 27.87 % in B-type vacuoles. Second, the largest increase in read number was observed for chloroplast rRNA species, accumulating 28.55% of all reads. Similarly, tRNA (15.36%) and mRNA (8.56%) revealed increased read numbers (Figure 2G). Small RNA types accumulate to 1.55% in sum. For details of read distributions please refer to Table S2.

AtRNS2-T-DNA insertion lines showed reduced vacuolar adenylate contents and activity.

RNS2 was identified as vacuolar RNase involved in a housekeeping function in RNA homeostasis. Knockout mutants of *RNS2* (*rns2-1* and *2-2*) have been described exhibiting RNA accumulation and constitutive autophagy (Hillwig et al., 2011; Floyd et al., 2012, 2017). However, the effect of a loss of RNS2 on vacuolar RNA composition and that of breakdown products and intermediates has not been analyzed so far. *Rns2-2* (SALK_069588) was described as real knockout line of *RNS2* but *rns2-1* as expressing an C-terminal truncated version of *RNS2* (Floyd et al., 2017). Therefore, we characterized another independent T-DNA insertion line, *rns2-3* (SAIL_338_G11). RT-PCR confirmed the production of a null mutant by T-DNA insertion (Figure S1). The level of autophagosomes in *rns2-2, rns2-3* was monitored by staining with monodansylcadaverine (MDC) of seedling roots and counting in the elongation zone as described before (Hillwig et al., 2011) and the number of autophagosomes was clearly increased in both lines compared to the wildtype (Figure 3A). Whereas WT roots showed 3.2 ± 0.6 autophagosomes per cell, in *rns2-2* and *rns2-3* the corresponding numbers were 6.8 ± 0.9 and 6.3 ± 0.8 (Figure 3A). This observation is in line with previous reports and corroborates *rns2-3* like the other RNS2 mutants exhibit constitutive autophagy. T2 type RNases typically cleave RNA in an endo-nucleolytic way, via the catabolic intermediates 2', 3'-cNMP and 3'NMP. When we incubated RNA with vacuolar content, both intermediates, here shown as 2',3'-cAMP and 3'AMP could be detected by HPLC Clearly, vacuolar content from *rns2-2* and *2-3*, normalized to the same activity of the vacuolar marker enzyme alpha mannosidase, produced significantly less breakdown products. Corresponding production of 2',3'-cAMP was reduced to 28% for *rns2-2* and

2-3, and adenosine to 23% and 37% for *rns2-2* and *2-3,* respectively (Figure 3B, C). From this reduced production a RNA hydrolytic activity of wildtype vacuolar content of 17 nmol RNA nucleotides h^{-1} was calculated (Figure 3D). Activity in vacuoles from *rns2-2* plants was reduced to 5 nmol RNA nucleotides h^{-1} and 7 nmol RNA nucleotides h^{-1} in *rns2-3* (Figure 3 D). When we inspected the contents of both breakdown products in freshly isolated vacuoles (R-type), a similar picture emerged. Here, the wildtype contents of 2',3'-cAMP was 69 ± 3.5 nmol U^{-1} mannosidase and only 13.2 ± 2.2 nmol U^{-1} mannosidase in *rns2-2* and 14.8 ± 5 nmol U^{-1} mannosidase in *rns2-3* (Figure 3 E). No detectable amounts of 3'-AMP or adenine appeared indicating the presence of vacuolar nucleotidase-activity and the absence of vacuolar nucleosidase activity. However, adenosine was found inside vacuoles, accumulating to 25,3 ± 3.7 nmol U^{-1} mannosidase in WT vacuoles and to only 13 ± 2.1 nmol in *rns2-2* and 11.7 ± 2.7 nmol in *rns2-3* vacuoles (Figure 3E).

Comparing the vacuolar RNome from ATG5 and RNS2 mutants

Because of its important role in vacuolar RNA metabolism, a RNS2 mutant (SALK_069588) was compared to wildtype control in respect to the composition of the vacuolar RNome. According to our current understanding, autophagy is the mechanism to deliver cellular macromolecules, damaged organelles and ribosomes to the vacuole for degradation. This involves proteins as well as RNA (Bassham & MacIntosh, 2017). ATG5 is a major constituent of the autophagy machinery in Arabidopsis, and thus we included a well characterized ATG5 T-DNA insertion mutant (SAIL_129_B07) in our analysis (Yoshimoto et al., 2009)

ATG5 knockout mutants are characterized by an altered metabolism in prolonged darkness, leading to the inability to survive several days of darkness. When we performed

such an experiment, ATG5 knockout plants did not survive a 6 days dark treatment, whereas wildtype and both RNS2 knockout mutants could recover completely (Figure 4A).

For the comparison of the vacuolar RNome, three rounds of vacuole (B-Type) isolations from wildtype and the three mutants (*rns2-2, rns2-3, atg5-1*) were performed. Whereas the purity, intactness and presence of RNA fragments inside vacuoles was shown before (Figure 2), we again compared these parameters for all vacuole isolation experiments. Although slight variations in those parameters occurred between biological replicates, overall no significant differences between vacuoles from different genotypes became apparent (Table S3). This also holds true for the extractable amount of RNA (Table S3). To check for the size distribution of RNAs from the three genotypes, Bioanalyzer runs on Pico-RNA chips were performed. The majority of RNAs showed a size of 25 to 200 nt in all three genotypes with only very few larger RNA species. However, no indication for the presence of intact ribosomal RNA (size > 1000nt) was found in any sample analyzed (Figure 4B). In addition, the RNA size profiles of all three genotypes were similar (Figure 4B).

After library preparation and sequencing as described above, between 22 M and 58 M reads were obtained (Table S3). Subsequently, adapter sequences were removed and sequences < 12 nt in size (< 13 nt for miRNAs) excluded from files used for mapping. Mapping was performed by as given in methods on the Araport11 genome assembly corrected by incompletely annotated ribosomal RNA species according to (Table S4).

A high number of reads accumulated on the cytosolic 45S rRNA gene and t-RNA genes. Comparing accumulated reads of the 45S rRNA gene illustrated a complete coverage of the gene with the exception of ITS1 and 2 regions (Figure S2). We interpret this as indication for a DNA free sample preparation (Figure S2). Furthermore, the read length

distribution markedly differed between ATG5 samples and both, wildtype and RNS2 samples (Figure S2).

A differential analysis with DeSeq2 comparing WT and ATG5 found 5080 gene loci with different read numbers out of a total of 29430 loci with mapped reads (Figure 4C). Similar numbers were obtained when comparing ATG5 and RNS2. However, only 65 gene loci differ between WT and RNS2 (Figure 4D) Detailed results from the differential analysis (p value <0.05) comparing the three genotypes can be found in Table S5.

A more detailed sample analysis revealed marked differences in photosynthesis related genes. Whereas , 37 corresponding chloroplast encoded gene products were 1.06 to 4.02 fold (log2) more abundant in WT vacuoles, 55 from 58 photosythesis associated nuclear genes (phang) were more abundant (1.11 to 5.77 fold (log2) in *atg5-1* ; Figure 4E).

Among the 65 gene loci differing between WT and RNS2 no phang or chloroplast encoded photosynthesis-related gene loci are present i.e. this observation was unique for the ATG5 samples (Table S5). Instead, mRNAs encoded by genes of functional categories “RNA metabolism” and “Protein degradation” were highly represented (Table S5). When inspecting unique reads, it appeared that *atg5-1* mutants accounted for only 5% of uniques reads whereas *rns2-2* and wt exhibited 15-20% unique reads (Figure 4F). This large proportion of missing reads could be attributed mainly to chlorolast genome encoded reads (Figure 4G).

Vacuoles contain intact miRNAs Micro RNAs (miRNAs) represent a class of small RNAs exhibiting regulatory functions in plant cells. As we identified these molecules in our vacuolar preparations we investigated these in more detail and extracted miRNA reads from mapping populations. The relative abundance of miRNAs in our libararies is low, usually below 2% of total reads which is drastically lower as one would expect from

cellular sRNA libraries which usually contain 50-80% miRNA reads, especially as we used 5´-monophosphate specific ligation which enriches for canonical miRNAs.

The median of read length of these miRNAs was 21nt for eight out of nine samples, only in case of *atg5-1* ,2 it was 20 nt, thus these reads match match the size of mature and functional miRNAs (Figure 5A). For most samples, 75% miRNA mapping reads were between 18 and 21 nt long indicating the presence of mature mRNAs instead of degradation products. These would be apparent in Fig. 5 A as our lenght trimming of reads still maintains reads above 15 nt. Only *atg5-1*,1 and 2 exhibited a slightly larger zone (Figure 5A).

A clustering analysis over all 427 miRNAs revealed reduced frequencies for all three ATG5 samples.his is illustrated by selected individual miRNAs miR166c, miR172c, miR156d-5P and miR159a (Figure5C). Although numerous miRNAs have been discovered in animals and plants, many of the corresponding functions in plants are only predicted (Yu et al., 2017). Among them is miR166c, which is predicted to target mRNAs coding for HD-Zip transcription factors and thereby regulating organ development and meristem maintenance (Rhoades et al., 2002). Another example is given by miR172c thought to target mRNAs of APETALA2-like transcription factors, thus influencing flowering and floral organ identity (Aukerman and Sakai, 2003). With miR156d, which is predicted to target mRNAs coding for Squamosa-promoter binding protein (SBP) box, we found a further representative of miRNAs modulating floral development (Cardon et al., 1997). MiR159a, predicted to target MYB transcription factors involved in defense and developmental mechanisms. Herein gibberellic acid and auxin mediated regulation in phosphate starvation and growth take place (Rhoades et al., 2002; Devaiah et al., 2009; Shin et al., 2007).**iscussion**

The presence of RNA in vacuoles and corresponding RNase activity is known since long (Boller & Kende, 1979; Abel et al. 1990; Bariola et al., 1999; Hillwig et al. 2011). More recently, RNA delivery to this compartment by autophagy received attention (Floyd et al., 2012; Ishida et al., 2014; Bassham & MacIntosh, 2017). In vacuoles from barley seedlings and Arabidopsis rosette leaves, isolated according to established protocols, evidence for the presence of (r)RNA was obtained by us using different techniques. 1. staining of RNA by Syto-RNA Select in intact vacuoles (Figure 1,2) 2. RNase treatment of isolated vacuoles clearly indicated that RNAs are located inside vacuoles as they were protected against enzymatic degradation. 3. Northern hybridization of RNA purified from intact vacuoles with rRNA specific probes. By this, small sized signals in the range of 20 to 120 nt were detected for vacuolar RNAs from Barley and Arabidopsis (Figure 1, 2).

Cloning of isolated vacuolar RNAs and Illumina sequencing allowed a genome wide identification of RNA reads and a quantification of these. When categorizing the mapped reads rRNAs were found being most prominent, making up to 92% of all reads found from vacuoles isolated according to Robert et al. (2007). Besides cytosolic rRNAs also chloroplastic (cp) rRNAs were found in differing amounts. In Barley, a similar picture emerged. 52% of the top 12 reads (accounting for 71% of all reads) mapped to the chloroplast 16S rRNA. Furthermore, 7 photosynthesis associated nuclear genes (phang) were identified (12%). This is similar to our results for Arabidopsis. The identification of cell walls associated hydrolases might be more specific for cereal species. Comparing two vacuole isolation protocols, we found that R-Type vacuoles contained only little cp rRNA (6%), whereas B-type vacuoles contained 29% cp rRNA. Barley and R-Type vacuoles were isolated from developing leaves, in contrast, B-type vacuoles were obtained from fully developed, mature leaves. It can be assumed that mature leaves exhibit higher rRNA turnover and contain more aged or damaged chloroplasts prone to

degradation (Woodson et al., 2015). Autophagy is a process involved in the degradation of cellular macromolecules and even organelles (MacIntosh & Bassham, 2011; Floyd et al., 2012; Floyd et al., 2015, Bassham & MacIntosh, 2017). This includes Rubisco-containing bodies (RCBs), ATI1-PS (ATG8-interacting Protein 1) bodies, and small starch-like granule (SSLG) bodies (Ishida et al., 2014, Otegui, 2017). In addition, autophagy independent degradation of damaged chloroplasts has been reported (Wang and Blumwald, 2014, Woodson et al., 2015). Both pathways, autophagy dependent and independent may contribute to the observed accumulation of RNAs in vacuoles. Besides rRNA other types like t-RNAs, mRNAs and small RNAs (miRNA, snRNA, snoRNA, ncRNA) were found in our analysis. Overall, this clearly points to plants operating a bulk transport of RNA species to the vacuole.

RNS2 was identified as vacuolar RNase of Arabidopsis and corresponding knockout lines were shown to exhibit a longer rRNA half life and constitutive autophagy (Hillwig et al., 2011). In our analysis of two independent RNS2 T-DNA insertion lines we could confirm the presence of an increased autophagosome number in corresponding root cells. At the same time, RNA degradation products were decreased in these lines, as well as the extractable vacuolar RNase activity. However, about 30% of residual RNase activity was found in both RNS2 knockout lines, in line with similar observations by others (Floyd et al., 2017). This provides evidence for the presence of further RNases in Arabidopsis vacuoles. It was expected to find a higher percentage of non degraded RNAs in RNS2 knockout mutants (Bassham & MacIntosh, 2017). However, when we analysed the size of isolated RNAs no difference to wildtype controls or ATG5 mutants became obvious. In addition to our comparison of vacuolar RNA contents between RNS2 and wildtype plants, only 65 genes were identified with significantly altered mapped reads. However, almost no alteration in the read length profile of mapped reads at highly covered loci was

observed. We explain the finding of an overall similar RNA size, read profile and RNA composition by a compensatory function of further, so far unknown vacuolar RNases.

In contrast to the minor impact of RNS2 on vacuolar RNA composition, ATG5 showed a huge effect. ATG5 is a main component of the Arabidopsis autophagy system conjugating to ATG12, a ubiquitin like protein tag. The ATG5-ATG12 conjugate is required for autophagosome formation, closure and transfer to the vacuole (Thompson et al., 2005; Le Bars et al., 2014). In line with this, fewer autophagosomes were identified by MDC labelling in *atg5-1* (Minina et al., 2018) and these mutants are characterized by a massive carbon starvation phenotype and early senescence. When grown on soil, they cannot survive a 5-6 day dark-induced carbon starvation (Figure 4; Thompson et al., 2005). Under the same conditions, the effect on wildtype as well as on RNS2 mutants was small. When the RNA composition of *atg5-1* was compared to wildtype, a large amount of genes with altered read number were found. A detailed analysis revealed that most of these reads mapped to the chloroplast chromosome (Figure 4 D). This might be explained by a high selectivity of ATG5 related autophagy for chloroplast RNA. However, as *atg5-1* does not accumulate autophagosomes, the question about the fate of chloroplast RNA in this mutant remains. At least four pathways for the degradation of Chloroplasts or parts thereof exist, 1. Chlorophagy, 2. Piecemeal autophagy leading to formation of rubisco containing bodies (RCB), 3. Chloroplast vesiculation (CV), and 4. the formation of senescence associated vacuoles (SAV). Chlorophagy functions in analogy to mitophagy, describing the selective elimination of dysfunctional mitochondria in yeast and mammals (Kanki et al., 2015). Similarly chlorophagy can remove entire damaged chloroplasts. Due to photodamage, these chloroplasts were found in wildtype vacuoles, but accumulated in the cytoplasm of ATG mutants (Izumi et al., 2017). The RCB pathway mobilized stromal proteins to the vacuole (Izumi et al., 2018) and both

pathways are autophagy dependent (Izumi et al., 2015, 2017). It is therefore unlikely they play roles in *atg5-1* plants. In contrast, CV represents an autophagy independent way to deliver chloroplast contents to the vacuole in form of small vesicles (Wang and Blumwald, 2014). A second autophagy independent pathway is defined by SAV Formation. SAV's represent an independent lytic compartment that does not require fusion with the central lytic vacuole (Martinez et al., 2008, Xie et al., 2015). If SAV is favoured in Atg5 plants, we are blind for RNA, which is incorporated in SAVs. Indeed chloroplasts were lost faster in *atg5-1* plants and it was thus supposed this was based on the activation of alternative, autophagy independent breakdown routes (Thompson et al., 2005). CV and SAV might be good candidates for such alternative routes. However, to the best of our knowledge for none of the before discussed chloroplast degradation pathways RNA has been identified as a target. Therefore, it is hard to predict whether chloroplast RNA breakdown involves CV or SAV or so far unknown, RNA specific pathways.

Next to the smaller fragments of longer RNAs which are likely degradation products, we also detected miRNA reads. Surprisingly, the read length of vaculoar miRNAs is similar to that of mature plant miRNAs, indicating that these are nor degradet but rather being intact molecules.

In general, miRNAs play important regulatory role in plant developmental processes and the response to nutrient starvation by acting on transcription factors (Rajagopalan, 2006). In mammals autophagy itself is target of regulation by miRNAs. (Yang et al., 2019). Such regulation has so far not be identified for plants. The median read length of vacuolar miRNAs was 21 nt in eight out of nine samples, matching exactly the typical length of mature, functional miRNAs. Supposedly, miRNAs are prone to degradation in vacuole by autophagy (Yu et al., 2017). This might explain the reduced frequency of miRNAs

found in ATG5 plants. However, the question appears why intact, mature miRNAs dominate in vacuoles. It is known that miRNAs circulating in the blood stream of mammals are surprisingly stable, possibly by a permanent protection against RNAse by Argonautes. In plants, the presence of Ago in vacuoles in not known, and we cannot explain right now the biological significance of vacuolar miRNAs. They may represent a reservoir for regulatory miRNAs and could be involved in regulation of plant circulating sRNAs. However, the vacuole itself appears to hold more RNA secretes than just serving as a compartment for their degradation.

Methods

Plants used for analysis and growth conditions

We used wildtype Columbia Arabidopsis plants and T-DNA-insertions lines for *RNS2* (At2g39780) and *ATG5* (At5g17290). These were SALK_069588 (*rns2-2*) SAIL_338_G11 (*rns2-3*) and SAIL_129_b07 (*atg5-1;* Yoshimoto et al., 2009, Alonso et al., 2003, Sessions et al., 2002). Barley (*Hordeum vulgare* type "Barke") seeds were a gift from Breun Saatzucht (Herzogenaurach, Germany). *Arabidopsis thaliana* (L.) Heynh. plants (ecotype Columbia) were grown in standardized ED73 (Einheitserde und Humuswerke Patzer, Buchenberg, Germany) soil grown at 120 µmol quanta m^{-2} s^{-1} in a 10 h light/14 h dark regime (short day), temperature 22°C, humidity 60%). Prior to germination, seeds were incubated for 24 h in the dark at 4°C for imbibition. Barley was grown in the same soil under the same growth conditions. RNS2-3 T-DNA insertion mutant analysis as given in Figure S1 was performed with primers listed in Table S6.

Vacuole isolation

The isolation of *H. vulgare* vacuoles was performed similar to the protocol from Rentsch & Martinoia (1991) with modifications in (Tohge et al., 2011; Ramos et al., 2010). For the isolation primary leaves from 8-9 day old plants were harvested at the beginning of the light period. Isolated vacuoles were either used directly for experiments or frozen at -20 °C for later RNA isolation. The isolation of *A. thaliana* vacuoles (B-type) was performed according to the protocol of Burla *et al.* (2013). For this we used leaves of Arabidopsis plants singularized and grown under short day conditions for six weeks. The isolation of *A. thaliana* vacuoles (R-type) was performed according to the protocol of Robert *et al.* (2007). Arabidopsis seeds were sown in pots and grown without

singularizaton for 4 to 6 weeks under short day conditions. Plants were harvested before the onset of light.

RNA preparation

RNA was prepared from isolated vacuoles using **c**hloroform-phenol extraction (peqGOLD TriFast™ FL, Peqlab, Erlangen, Germany) according to the manufacturers advice. The reagent was directly added to frozen vacuoles to inhibit any RNase activity. To enhance RNA yields, glycogen (0.05 - 1 µg μl^{-1}) was added to the aqueous phase during subsequent precipitation with EtOH.

Labelling of nucleic acids

Probes for Northern hybridization were labelled with [α-^{32}P]-dCTP using Rediprime II (Amersham, Bucinghapshire, UK) according to the manufacturers instruction. Endlabeling of RNA was achieved with T4-polynukleotide kinase (New England Biolabs) For this, 10 µM RNA was incubated with 1 µl [γ-^{32}P]-ATP (150 µCi μl^{-1}), 1.5 µl T4-Polynukleotid-Kinase (10 U μl^{-1}) in reaction buffer for 1 h at 37 °C. Subsequently RNA was cleaned with QIAquick Nucleotide Removal-Kit (Qiagen, Hilden, Germany)

RNA was seperated on denaturing gels using formaldehyde (Northern blot, Sambrook et al., 1989) or on high resolution urea 17.5% polyacrylamide gels (PAGE, endlabeled RNA). Quantification was achieved with a MP Storage Phosphoscreen on a Cyclone Phospho-Imager (Perkin-Elmer,).

Enzyme activity and metabolite determination

Alpha mannosidase was quantified according to Pertl-Obermayer et al., (2016). Glycerinaldehyde-3-phosphate-dehydrogenase was determined as given in Stitt *et al.,* (1983), UDP-glucose-pyrophosphorylase according to Zrenner *et al.* (1993). Chromato-graphical analysis of adenylates was performed as given in Daumann et al. (2018).

Quantification of autophagosomes

Autophagosomes were quantified as given in Floyd et al. (2015). For each plant line a minimum of 70 cells were insepected. Microscopic analysis was done with a Leica SP5II confocal laser scanning microscope (Leica microsystems, Mannheim, Germany). The following settings were used: (488-nm excitation and 50- to 560-nm detection of emission for SYTO RNA Select, 514-nm excitation and 714- to 754-nm detection of emission for FM4-64 and 405-nm excitation and 474- to 532nm emission wavelength for MDC (monodansyl cadaverine) through a HCX PL APO 63x1.2W water immersion objective).

Library preparation and Illumina sequencing

RNA libraries were prepared from 70ng vacuole RNA without further size exclusion. Using the „NEBNext® Multiplex Small RNA Library Prep Set for Illumina"-Kit (New England Biolabs, Ipswich, MA, USA) we used diluted adapters and 18 hours for 3´-adapter ligation at 16°C. After 15 PCR cycles, the library was purified from a 6% native TBE-PAGE. Library size and quantity was additionally determined using the Qubit Fluorometer and the Agilent Bioanalyzer DNA HS Chips. Illimina Sequencing was carried out on a HiSeq2500 platform (Libraries WT_1-3, ATG5-1_1-3, RNS2-2_1-3, referred to in Figure 4 and R-type Arabidopsis, B-type Arabidopsis, referred to in Figure) 2H using the RAPID mode for 50 cycles or the Illumina MiSeq (Barley library, referred to in Figure 1G) also for 50 cycles. Reads were demultiplexed and trimmed for adapters using Trim Galore which uses Cutadapt. We eliminated all reads shorter than 13nt, unless indicated otherwise

Data analysis

For comparison of R-type and B-type vacuolar RNA contents (Pie charts in Fig. 2G) individual reads were trimmed eliminating reads shorter than 15 nt and aligned using

HISAT2 with adapted parameters (-k 20; -secondary). Aligned reads were counted using multicov (bedtools). The percentage of counts for each RNA type was calculated based on the gene annotation.

Barley reads obtained from Illumna MySeq sequencing samples were trimmed eliminating reads shorter than 15 nt and aligned using Bowtie for Illumina from galaxy tools (Afgan et al., 2018). Counting was performed with htseq counts.

To analyse genotype specific differences in vacuolar RNA composition, reads were processed as follows. First, adapter trimming was performed using TrimGalore (v. 0.4.2, https://github.com/FelixKrueger/TrimGalore). Reads shorter than 13bp were discarded. Subsequently, reads were mapped against the reference genome using RNA STAR with a maximum intron size of 3000bp (v. 2.5.2b-0, Dobin et al. 2013) and quantified using htseq-count (v. 0.6.1, --m intersection-nonempty, Anders et al. 2015). Normalization and differential expression analysis among genotypes were carried out using DESeq2 (v. 2.11.40.6, Love et al. 2014). Gene enrichment analysis was calculated conducting a hypergeometric test (Rivals et al. 2007, doi: 10.1093/bioinformatics/btl633) using BioFSharp (v.0.1.0, https://github.com/CSBiology/BioFSharp). All Plots were generated using FSharp.Plotly (v. 1.1.1, https://github.com/muehlhaus/FSharp.Plotly).

For comparison of miRNAs the following procedure was applied. Reads were mapped with up to one mismatch against the reference genome using bowtie 1.2.2 (-a -v1 --best –strata). MiRNAs were quantified using featureCounts 1.5.2 and the annotations of Araport 11, while requiring an overlap of at least 80% of the read with the annotation. Fractional counts were assigned to reads mapping to multiple locations (-M --fractional). Counts were normalized to reads per million (RPM). Clustering of miRNAs was performed with hierarchical clustering using Euclidean distance and complete linkage, and performed on row-scaled RPM normalized counts, while considering only miRNAs

that were expressed with at least 5 reads in one sample. The analysis was performed with R 3.5.1 and the plots were generated with pheatmap 1.0.12 and ggplot2 3.1.0.

Author Contributions

Conceptualization: T.Mö., M.S., C.G., T.Mü, J.H.; Methodology, M.S., C.G., D.H. Investigation: D.H., F.D., C.G. (vacuole isolation, RNA isolation and library preparation) K.N. (Sequencing and Data handling) D.Z., J.H., T.Mü T.F., A. K. (Bioinfomatic and statistic Data analysis) T.Mö., C.G., D.H. wrote the manuscript.

Acknowledgements

The work was supported by the Forschungsinitiative Rheinland Pfalz (BioComp to T.M.) K.N. was supported by the NBI grant (031L0101D) from the Federal Ministry of Education and Research.

Conflict of interest: The authors declare no conflict of interest.

References

Abel, S., Blume, B., Glund, K. (1990) Evidence for RNA-oligonucleotides in plant vacuoles isolated from cultured tomato cells. *Plant Physiol.* 94: 1163-1171

Abel, S., Glund, K. (1986) Localization of RNA-degrading enzyme activity within vacuoles of cultured tomato cells. *Physiologia Plant.* 66: 79-86

Abel, S., Glund, K. (1987) Ribonuclease in plant vacuoles: purification and molecular properties of the enzyme from cultured tomato cells. *Planta* 172: 71-78

Afgan, E., Baker, D., Batut, B., van den Beek, M., Bouvier, D., Čech, M., Chilton, J., et al. (2018). The Galaxy platform for accessible, reproducible and collaborative biomedical analyses: 2018 update, *Nucleic Acids Res.* 46: 537–544

Alonso, J. M., Stepanova, A. N., Leisse, T. J., Kim, C. J., Chen, H., Shinn P. et al. (2003). "Genome-wide insertional mutagenesis of *Arabidopsis thaliana*." *Science* 301: 653-657.

Anders, S., Pyl, P. T., Huber, W. (2015). HTSeq—a Python framework to work with high-throughput sequencing data. *Bioinformatics* 31: 166-169.

Aukerman, M. J., Sakai, H. (2003). Regulation of flowering time and floral organ identity by a microRNA and its APETALA2-like target genes. *Plant Cell* 15: 2730-2741

Le Bars, R., Marion, J., Le Borgne, R., Satiat-Jeunemaitre, B., Bianchi, M. W. (2014). ATG5 defines a phagophore domain connected to the endoplasmic reticulum during autophagosome formation in plants. *Nature comm*. 5: 4121.

Bariola, P. A., MacIntosh G. C., Green P.J. (1999). Regulation of S-like ribonuclease levels in Arabidopsis. Antisense inhibition of RNS1 or RNS2 elevates anthocyanin accumulation. *Plant Cell Physiol*. 119: 331-342.

Bassham DC, MacIntosh, GC. (2017) Degradation of cytosolic ribosomes by autophagy-related pathways. *Plant Sci.* 262: 169-174

Bernard C, Traub M, Kunz HH, Hach S, Trentmann O, Möhlmann T. (2011) Equilibrative nucleoside transporter 1 (ENT1) is critical for pollen germination and vegetative growth in Arabidopsis. *J. Exp. Bot*. 62: 4627-37

Boller, T., Kende, H. (1979) Hydrolytic enzymes in the central vacuole of plant cells. *Plant Physiol.* 63: 1123-1132

Burla, B., Pfrunder, S., Nagy, R., Francisco, R. M., Lee, Y., Martinoia, E. (2013) Vacuolar transport of abscisic acid glucosyl ester is mediated by ATP-binding cassette and proton-antiport mechanisms in Arabidopsis. *Plant Physiol.* 163: 1446-1458

Cardon, G. H., Höhmann, S., Nettesheim, K., Saedler, H., Huijser, P. (1997). Functional analysis of the *Arabidopsis thaliana* SBP-box gene SPL3: a novel gene involved in the floral transition. *Plant J.* 12: 367-377.

Daumann M, Hickl D, Zimmer D, De Tar RA, Kunz H-H, Möhlmann T (2018) Characterization of filament-forming CTP synthases from Arabidopsis thaliana. *Plant J.* 96, 316-328

Devaiah, B. N., Madhuvanthi, R., Karthikeyan, A. S., Raghothama, K. G. (2009). Phosphate starvation responses and gibberellic acid biosynthesis are regulated by the MYB62 transcription factor in Arabidopsis. *Mol. Plant* 2: 43-58.

Dobin, A., Davis, C. A., Schlesinger, F., Drenkow, J., Zaleski, C., Jha, S. et al. (2013). STAR: ultrafast universal RNA-seq aligner. *Bioinformatics* 29: 15-21.

Floyd, B. E., Morriss, S. C., MacIntosh, G. C., Bassham, D. C. (2012). What to Eat: Evidence for Selective Autophagy in Plants *F. J. Int. Plant Biol.* 54: 907-920.

Floyd, B. E., Morriss, S. C., MacIntosh, G. C., Bassham, D. C. (2015). Evidence for autophagy-dependent pathways of rRNA turnover in Arabidopsis. *Autophagy* 11*:* 2199-2212.

Floyd, B. E., Mugume, Y., Morriss, S. C., MacIntosh, G. C., Bassham, D. C. (2017). Localization of RNS2 ribonuclease to the vacuole is required for its role in cellular homeostasis. *Planta* 245: 779-792.

Hedrich, R., Sauer, N., Neuhaus, H.E. (2015) Sugar transport across the plant vacuolar membrane: nature and regulation of carrier proteins. *Curr. Opin. Plant Biol.* 25: 63-70

Hillwig, M. S., Contento, A. L., Meyer, A., Ebany, D., Bassham, D. C., MacIntosh, G. C. (2011) RNS2, a conserved member of the RNase T2 family, is necessary for ribosomal RNA decay in plants. *Proc. Natl. Acad. Sci. USA* 108: 1093-1098

Huang, H., Kawamata, T., Horie, T., Tsugawa, H., Nakayama, Y., Ohsumi, Y., Fukusaki, E. (2014) Bulk RNA degradation by nitrogen starvation-induced autophagy in yeast. *EMBO J*: e201489083.

Ishida, H., Izumi, M., Wada, S., Makino, A. (2014). Roles of autophagy in chloroplast recycling. *BBA-Bioenergetics* 1837: 512-521.

Izumi, M., Ishida, H., Nakamura, S., Hidema, J. (2017). Entire photodamaged chloroplasts are transported to the central vacuole by autophagy. *Plant Cell* 29: 377-394.

Izumi, M., Nakamura, S. (2018). Chloroplast protein turnover: the influence of extraplastidic processes, including autophagy. *Int. J. Mol. Sci.* 19: 828.

Kanki, T., Furukawa, K., Yamashita, S. I. (2015). Mitophagy in yeast: molecular mechanisms and physiological role. *BBA-Mol. Cell Res.* 1853*:* 2756-2765.

Love, M. I., Huber, W., Anders, S. (2014). Moderated estimation of fold change and dispersion for RNA-seq data with DESeq2. *Genome biol.* 15: 550.

MacIntosh, G. C., Bassham, D. C. (2011) The connection between ribophagy, autophagy and ribosomal RNA decay. *Autophagy* 7: 662-663.

Martínez, D. E., Costa, M. L., Gomez, F. M., Otegui, M. S., Guiamet, J. J. (2008). Senescence-associated vacuoles are involved in the degradation of chloroplast proteins in tobacco leaves. *Plant J*. 56: 196-206.

Michaeli, S., Honig, A., Levanony, H., Peled-Zehavi, H., Galili, G. (2014) Arabidopsis ATG8-Interacting protein 1 is involved in autophagy-dependent vesicular trafficking of plastid proteins to the vacuole. *Plant Cell* 26: 4084-4101

Minina, E. A., Moschou, P. N., Vetukuri, R. R., Sanchez-Vera, V., Cardoso, C., Liu, Q., ... & Marmon, S. (2018). Transcriptional stimulation of rate-limiting components of the autophagic pathway improves plant fitness. *J. Exp. Bot.* 69: 1415-1432.

Otegui, M. S. (2017). Vacuolar degradation of chloroplast components: autophagy and beyond. *J. Exp. Bot*. 69: 741-750.

Pertl-Obermeyer H, Duscha K, Trentmann O, Neuhaus HE, Schulze WX (2016) Quantitation of vacuolar sugar transporter abundance changes using QconCAT synthtetic peptides. *Front. Plant Sci.* 7:411. doi: 10.3389/fpls.2016.00411

Robert, S., Zouhar, J., Carter, C., Raikhel, N. (2007) Isolation of intact vacuoles from Arabidopsis rosette leaf-derived protoplasts. *Nat. Protoc.* 2: 259-262

Rajagopalan, R., Vaucheret, H., Trejo, J., Bartel, D. P. (2006). A diverse and evolutionarily fluid set of microRNAs in Arabidopsis thaliana. *Genes & development*, 20: 3407-3425.

Ramos M. S., Abele R., Nagy R., Grotemeyer M. S., Tampé R., Rentsch D., Martinoia E. (2010) Characterization of a transport activity for long-chain peptides in barley mesophyll vacuoles. *J.Exp. Bot.* 62: 2403–2410

Rentsch D., Martinoia E. (1991) Citrate transport into barley mesophyll vacuoles – comparison with malate-uptake activity. *Planta* 184: 532–537

Rhoades, M. W., Reinhart, B. J., Lim, L. P., Burge, C. B., Bartel, B., Bartel, D. P. (2002). Prediction of plant microRNA targets. *Cell* 110: 513-520

Rivals, I., Personnaz, L., Taing, L., & Potier, M. C. (2006). Enrichment or depletion of a GO category within a class of genes: which test? *Bioinformatics* 23: 401-407.

Sambrook, J., Fritsch, E. F. & Maniatis, T. (1989) *Molecular cloning*, Cold spring harbor laboratory press, New York.

Shin, R., Burch, A. Y., Huppert, K. A., Tiwari, S. B., Murphy, A. S., Guilfoyle, T. J., Schachtman, D. P. (2007). The Arabidopsis transcription factor MYB77 modulates auxin signal transduction. *Plant Cell* 19: 2440-2453.

Stitt, M., Wirtz, W., Heldt, H. W. (1983) Regulation of sucrose synthesis by cytoplasmic fructosebisphosphatase and sucrose phosphate synthase during photosynthesis in varying light and carbon dioxide. *Plant Physiol*. 72: 767-774

Sessions, A., E. Burke, G. Presting, G. Aux, J. McElver, D. Patton et al. (2002). A high-throughput Arabidopsis reverse genetics system. *Plant Cell* 14: 2985-2994.

The international barley sequencing consortium (2012) A physical, genetic and functional sequence assembly of the barley genome. *Nature* doi: 10.1038/nature11543.

Thompson, A. R., Vierstra, R. D. (2005) Autophagic recycling: lessons from yeast help define the process in plants. *Curr. Opin. Plant Biol* 8: 165-173

Trentmann, O., Neuhaus, H.E. (2014) Regulation of transport processes across the tonoplast membrane. *Front. Plant Sci.* doi: 10.3389/fpls.2014.00460

Tohge T., Ramos M. S., Nunes-Nesi A., Mutwil M., Giavalisco P., Steinhauser D., Schellenberg M., Willmitzer L., Persson S., Martinoia E., Fernie A. R. (2011) Toward the storage metabolome: Profiling the Barley vacuole. *Plant Physiol.* 157: 1469–1482

Wang, S., Blumwald, E. (2014) Stress-Induced Chloroplast Degradation in *Arabidopsis* is regulated via a process independent of autophagy and senescence-associated vacuoles. *Plant Cell* 26: 4875-4888.

Woodson, J. D., M. S. Joens, A. B. Sinson, J. Gilkerson, P. A. Salomé, D. Weigel, J. Fitzpatrick, A. Chory, J. (2015). Ubiquitin facilitates a quality-control pathway that removes damaged chloroplasts. *Science* 350: 450-454.

Xie, Q., Michaeli, S., Peled-Zehavi, H., Galili, G. (2015). Chloroplast degradation: one organelle, multiple degradation pathways. *Trends Plant Sci.* 20: 264-265

Yang M, Bu F, Huang W Chen L (2019) Multiple Regulatory Levels Shape Autophagy Activity in Plants. *Front. Plant Sci.* 10: 532. doi: 10.3389/fpls.2019.00532

Yoshimoto, K., Jikumaru, Y., Kamiya, Y. Kusano, M., Consonni, C., Panstruga, et al. (2009). Autophagy Negatively Regulates Cell Death by Controlling NPR1-Dependent Salicylic Acid Signaling during Senescence and the Innate Immune Response in Arabidopsis. *Plant Cell* 21: 2914-2927.

Yu, Y., Jia, T., Chen, X. (2017). The 'how'and 'where'of plant microRNAs. *New Phytol.* 216: 1002-1017.

Zrenner, R., Willmitzer, L. Sonnewald, U. (1993) Analysis of the expression of potato uridinediphosphate-glucose pyrophosphorylase and its inhibition by antisense RNA. *Planta* 190: 247-252.

Supplemental information:

Table S1:	Read distribution *Hordeum vulgare*
Table S2:	Read distribution of Arabidopsis R-type and B-type vacuoles
Table S3:	Comparison of "workflow parameters" *wildtype*, *rns2* and *atg5* RNome analysis
Table S4:	Araport11 Arabidopsis genome change log
Table S5:	DeSeq results comparing *wildtype*, *rns2* and *atg5* RNnome
Table S6:	Primers used
Figure S1:	*rns2-3* T-DNA insertion mutant analysis
Figure S2:	read profiles from 45S rDNA region

Figure legends:

Figure 1. Isolated rRNA from barley vacuoles with 25 to 200 nt in size is qualitatively classified. (**A**) Vacuoles were isolated from 8-9 day old *Hordeum vulgare* plants at the beginning of the light period. Microscopical inspection showed pure vacuoles without contaminating protoplasts. (**B-D**) RNA inside the vacuolar lumen was detected by incubation with SYTO® RNASelect™ Green Fluorescent cell stain (B). Brightfield image (C) shows vacuolar intactness and the overlay image (D) reveals RNA fluorescence only from the inside of the vacuole. Tonoplast is indicated by arrowhead (C and D; scale bar = 10 µm). (**E**) Separated RNA was blotted on a nylon membrane and hybridized with 5S rRNA and 18S rRNA probes. (**F**) Total RNA isolated from vacuoles was run on a Agilent RNA Pico Chip. The single peak with a width of 20 to 27 seconds at its base represents eluting RNA fragments with a size of 25 to 200 nt. (**G**) Illumina sequencing enabled classification of RNA species, with 75 % cytosolic and 5.8 % chloroplastic rRNA.

Fig. 2. Purity, intactness and RNA composition of R and B-Type vacuoles from arabidopsis. Plants were grown on soil for 4 to 6 weeks with dense sowed seeds for isolation of R-type vacuoles and 3 to 4 plants per pot for isolation of B-type vacuoles. (**A**) R-type and B-type vacuoles are almost free of extravacuolar contaminations. Marker enzyme activity was used for verification of plastidic (Glycerine aldehyd-3-phosphate dehydrogenase (GAPDH)) or cytosolic contamination (Uridine diphosphate glucose pyrophosphorylase (UGPase)). Enzymatic activity in protoplasts was used as control and set to 100%. (**B**) Tonoplast protects vacuolar RNA against extravacuolar RNase activity. Intravacuolar RNA from B-type vacuoles was stained with the RNA specific dye SYTO® RNASelect™ (green), whereas the tonoplast was visualized by the lipophilic dye FM4-64 (red). Treatment with RNase prior to staining had no influence on RNA signal (right; scale bar = 4 µm). (**C**) RNA from R-type vacuoles was non treated (lane 1), with Rnase at 10 µg ml^{-1} (lane 2), 0.5 mg ml^{-1} (lane 3) and during cell lysis while preparation with 10 µg ml^{-1} RNase A treated (lane 4). Afterwards RNA was radioactive endlabelled and separated by RNA-PAGE. For size determination 29 nt, 48 nt, 75 nt and 380 nt marker oligos were run on the same gel. Excessive free [γ-^{32}P]-ATP is indicated by arrowhead. (**D-F**) B-type vacuoles were non treated (D) or incubated for 1 h with 10 µg ml^{-1} RNase

A, followed by 1 h incubation with 400 µg ml^{-1} Proteinase K (E). Isolated RNA was separated on RNA chip. RNase A activity was verified by 15 min incubation of 10 µg ml^{-1} RNase A with 400 ng protoplastic RNA (F). (**G**) Illumina sequencing and mapping enabled classification of RNA species. RNA composition in R- and B-type vacuoles differs markedly in plastidic rRNA, t-RNA and mRNA content.

Fig. 3. T2 type RNase breakdown products are reduced in RNS2-2 and RNS2-3 mutant plants. (**A**) *rns2-2* and *rns2-3* exhibit constitutive autophagy. Seedling roots were stained with 0.05 mM monodansylcadaverine (MDC) in PBS for 10 minutes. Observed autophagosomes were counted within elongation zone. (**B-D**) RNA was incubated with vacuolar content from wt and *RNS2* mutants. Produced adenine derivatives 2',3'-cAMP (B) and adenosine (C) were quantified by HPLC and normalized to the vacuolar marker enzyme α mannosidase. (D) By this RNA hydrolysis activity was calculated. (E) Contents of adenosine and 2',3'-camp were quantified in different genotypes.

Fig. 4. Chloroplast encoded photosynthesis related gene products are strongly decreased in ATG5 vacuoles. (**A**) ATG5 plants are inable to cope with dark induced carbon starvation. Eight week old plants, grown under short day conditions (10 h light, 14 h dark), were transferred to complete darkness for 6 days. Replacing the plants to light recovered wildtype, *rns2-2* and *rns2-3*, but not *atg5-1* plants. (**B**) RNA isolated from B-type vacuoles is 25 to 200 nt in size. No alterations were observed in *atg5-1* and *rns2-2*. (**C-D**) Dseq analysis revealed significant differences (p value <0.05) in read numbers of 5080 mapped loci when comparing *atg5-1* to WT (red dots, C), whereas only 65 mapped loci were significantly altered in read numbers when comparing *rns2-2* to WT (D). (**E**) Photosynthesis related nuclear genes (Phang) were more abundant in ATG5, but photosynthesis related chloroplast encoded genes were less abundant compared to wildtype. (**F**) Percentage of unique reads in wildtype, RNS2-2 and ATG5. (**G**) Chloroplast encoded gene products are markedly decreased in RNA isolated from ATG5 vacuoles.

Fig. 5. Analysis of miRNAs found in vacuoles from the three different genotypes. (**A**) Size distribution of miRNA mapping reads. A median length of 21nt was observed for most samples. (**B**) Cluster analysis of miRNAs indicated lower amounts in ATG5

mutant plants. (**C**) typical examples of miRNAs with different frequencies in *atg5-1*, *rns2-2* and WT plants.

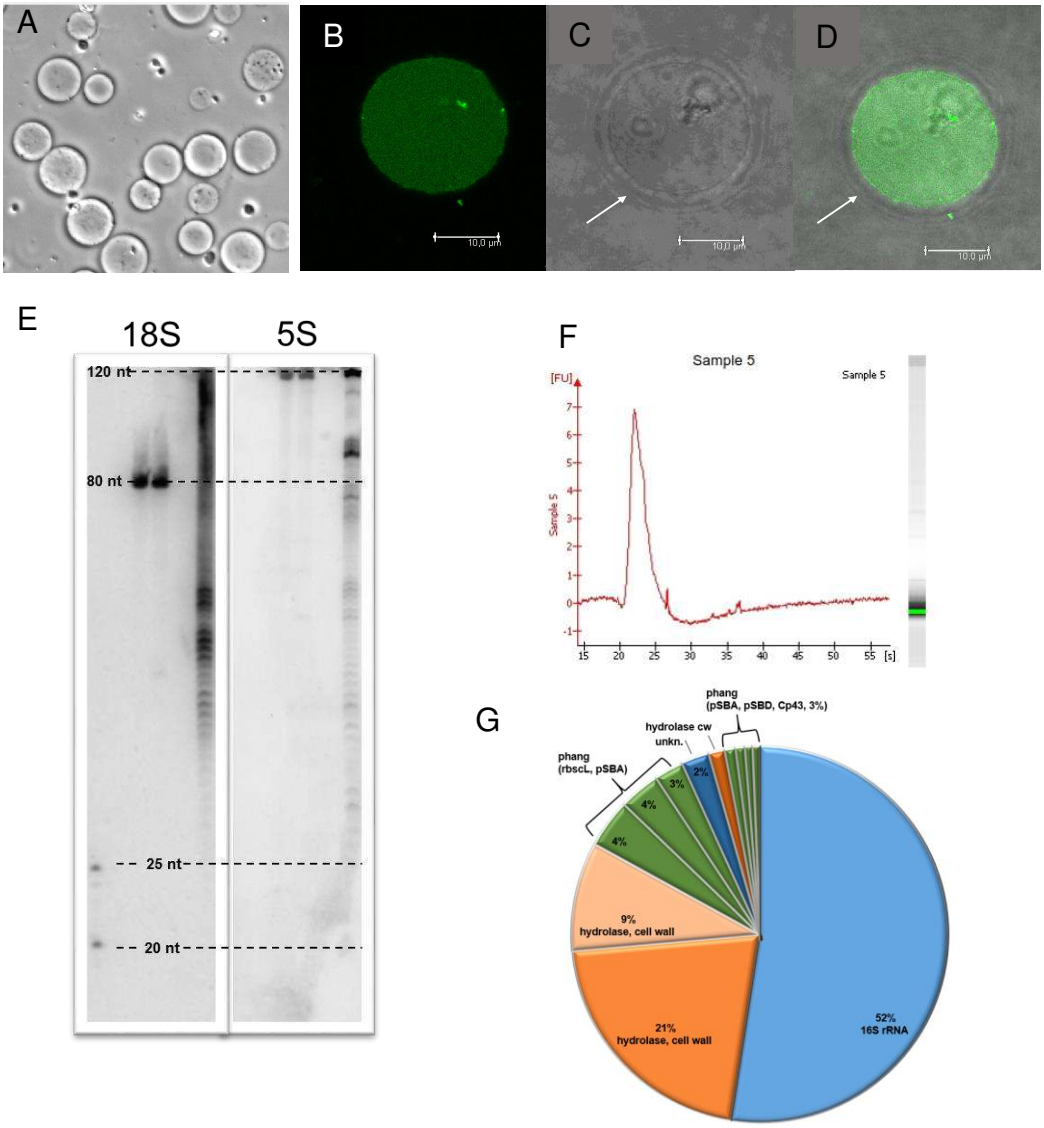

Fig. 1. Isolated rRNA from barley vacuoles with 25 to 200 nt in size is qualitatively classified. (**A**) Vacuoles were isolated from 8-9 day old *Hordeum vulgaris* plants at the beginning of the light period. Microscopical inspection showed pure vacuoles without contaminating protoplasts. (**B-D**) RNA inside the vacuolar lumen was detected by incubation with SYTO® RNASelect™ Green Fluorescent cell stain (B). Brightfield image (C) shows vacuolar intactness and the overlay image (D) reveals RNA fluorescence only from the inside of the vacuole. Tonoplast is indicated by arrowhead (C and D; scale bar = 10 µm). (**E**) Separated RNA was blotted on a nylon membrane and hybridized with 5S rRNA and 18S rRNA probes. **F**) Total RNA isolated from vacuoles was run on a Agilent RNA Pico Chip. The single peak with a width of 20 to 27 seconds at its base represents eluting RNA fragments with a size of 25 to 200 nt. (**G**) Illumina sequencing enabled classification of RNA species. Top 12 identified genes are shown with % frequency of reads. Photosynthesos associated nuclear genes (phang).

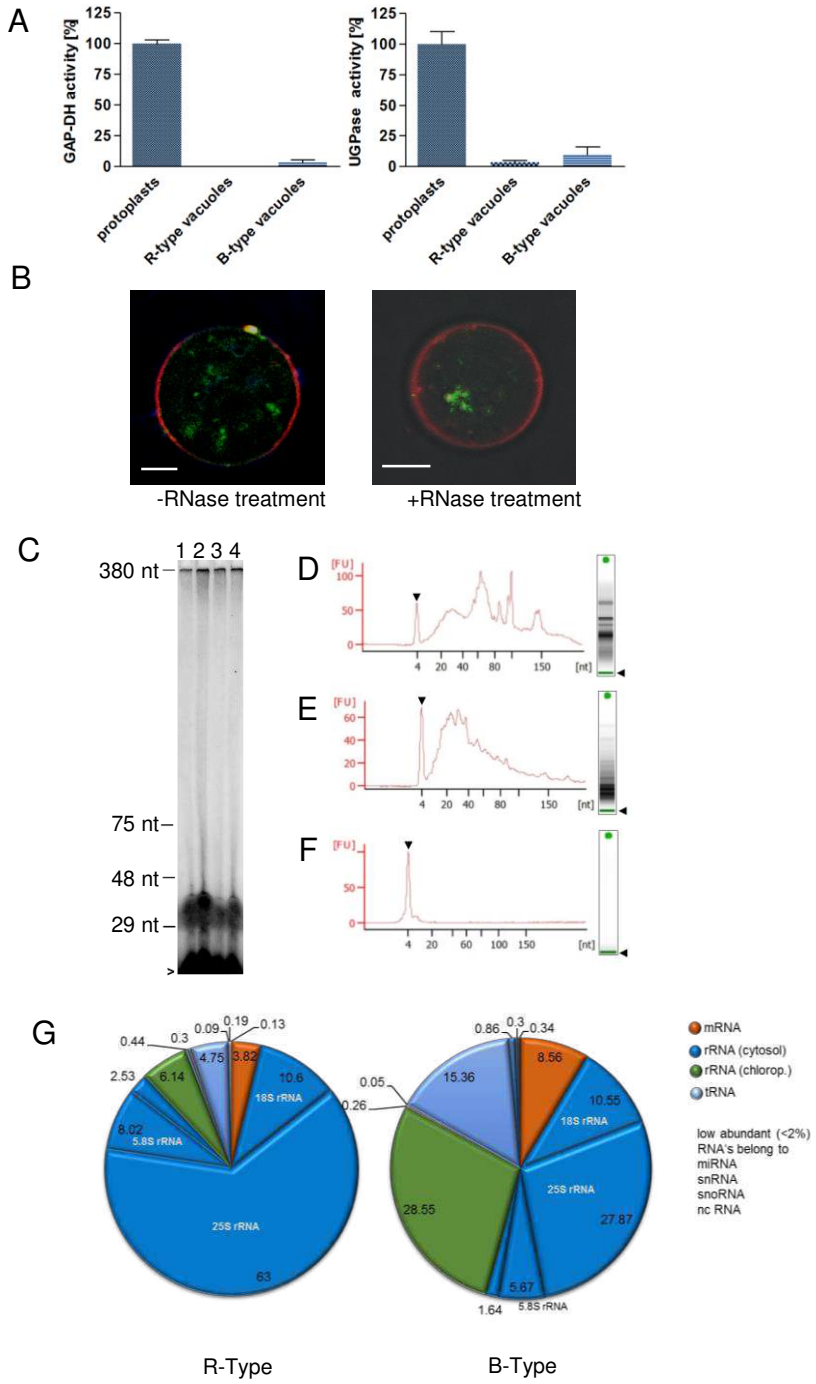

Fig. 2. Purity, intactness and RNA composition of R and B-Type vacuoles from arabidopsis. Plants were grown on soil for 4 to 6 weeks with dense sowed seeds for isolation of R-type vacuoles and 3 to 4 plants per pot for isolation of B-type vacuoles. (**A**) R-type and B-type vacuoles are almost free of extravacuolar contaminations. Marker enzyme activity was used for verification of plastidic (Glycerine aldehyd-3-phosphate dehydrogenase (GAPDH)) or cytosolic contamination (Uridine diphosphate glucose pyrophosphorylase (UGPase)). Enzymatic activity in protoplasts was used as control and set to 100%. (**B**) Tonoplast protects vacuolar RNA against extravacuolar RNase activity. Intravacuolar RNA from B-type vacuoles was stained with the RNA specific dye SYTO® RNASelect™ (green), whereas the tonoplast was visualized by the lipophilic dye FM4-64 (red). Treatment with RNase prior to staining had no influence on RNA signal (right; scale bar = 4 µm). (**C**) RNA from R-type vacuoles was non treated (lane 1), with 10 µg ml^{-1} (lane 2), 0.5 mg ml^{-1} (lane 3) and during cell lysis while preparation with 10 µg ml^{-1} RNase A treated (lane 4). Afterwards RNA was radioactive endlabelled and separated by RNA-PAGE. For size determination 29 nt, 48 nt, 75 nt and 380 nt marker oligos were run on the same gel. Excessive free [γ-^{32}P]-ATP is indicated by arrowhead. (**D-F**) B-type vacuoles were non treated (D) or incubated for 1 h with 10 µg ml^{-1} RNase A, followed by 1 h incubation with 400 µg ml^{-1} Proteinase K (E). Isolated RNA was separated on RNA chip. RNase A activity was verified by 15 min incubation of 10 µg ml^{-1} RNase A with 400 ng protoplastic RNA (F). (**G**) Illumina sequencing and mapping enabled classification of RNA species. RNA composition in R- and B-type vacuoles differs in plastidic rRNA, t-RNA and mRNA content.

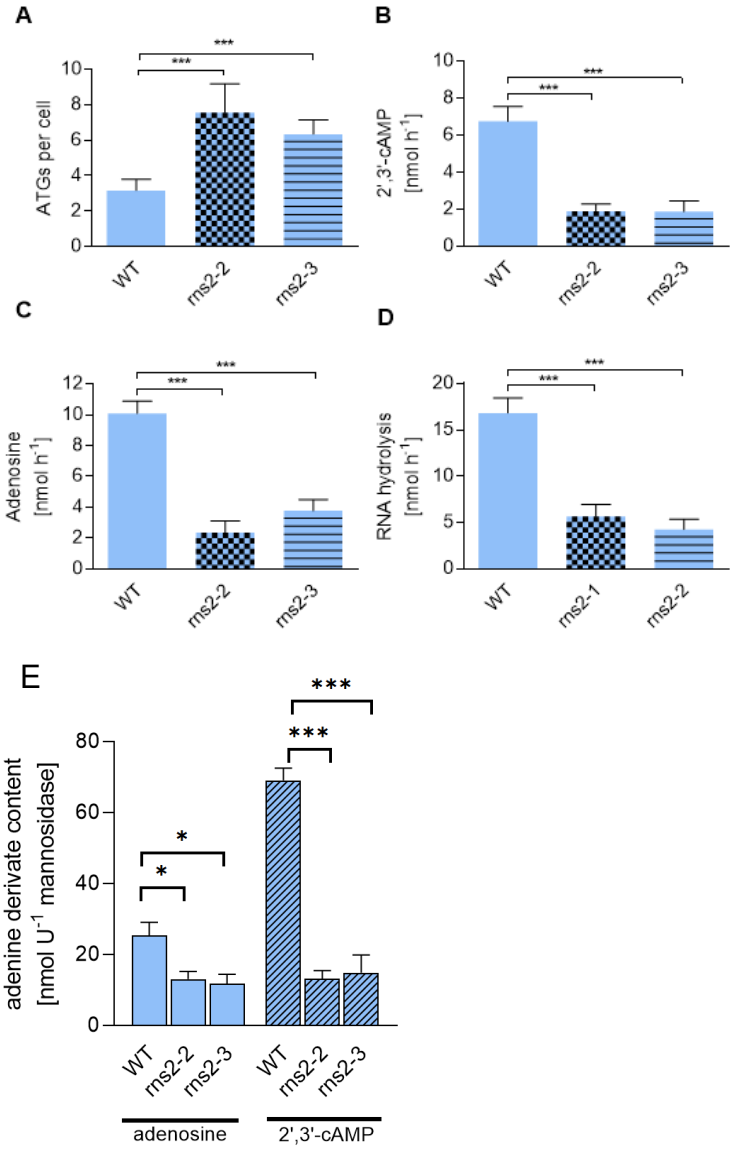

Fig. 3. T2 type RNase breakdown products are reduced in RNS2-2 and RNS2-3 mutant plants. (**A**) RNS2-2 and RNS 2-3 exhibit constitutive autophagy. Seedling roots were stained with 0.05 mM monodansylcadaverine (MDC) in PBS for 10 minutes. Observed autophagosomes were counted within elongation zone. (**B-D**) RNA was incubated with vacuolar content from wt and *RNS2* mutants. Produced adenine derivatives 2',3'-cAMP (B) and adenosine (C) were quantified by HPLC and normalization to vacuolar marker enzyme α mannosidase . (D) By this RNA hydrolysis activity was calculated. (E) Contents of adenosine and 2',3'-camp were quantified in different genotypes.

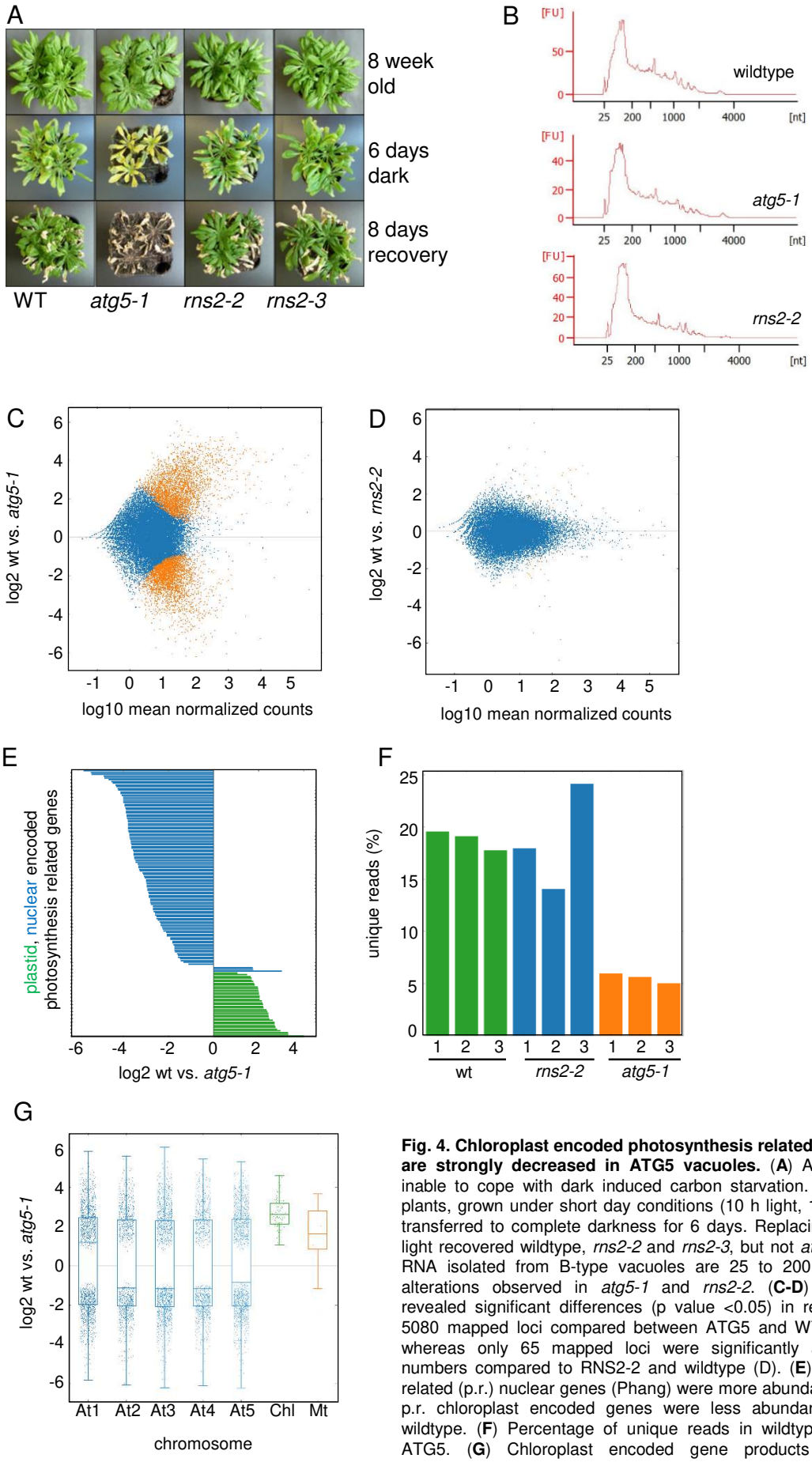

Fig. 4. Chloroplast encoded photosynthesis related gene products are strongly decreased in ATG5 vacuoles. (**A**) ATG5 plants are inable to cope with dark induced carbon starvation. Eight week old plants, grown under short day conditions (10 h light, 14 h dark), were transferred to complete darkness for 6 days. Replacing the plants to light recovered wildtype, *rns2-2* and *rns2-3*, but not *atg5-1* plants. (**B**) RNA isolated from B-type vacuoles are 25 to 200 nt in size. No alterations observed in *atg5-1* and *rns2-2*. (**C-D**) Dseq analysis revealed significant differences (p value <0.05) in read numbers of 5080 mapped loci compared between ATG5 and WT (red dots, C), whereas only 65 mapped loci were significantly altered in read numbers compared to RNS2-2 and wildtype (D). (**E**) Photosynthesis related (p.r.) nuclear genes (Phang) were more abundant in ATG5, but p.r. chloroplast encoded genes were less abundant compared to wildtype. (**F**) Percentage of unique reads in wildtype, RNS2-2 and ATG5. (**G**) Chloroplast encoded gene products are markedly decreased in RNA isolated from ATG5 vacuoles.

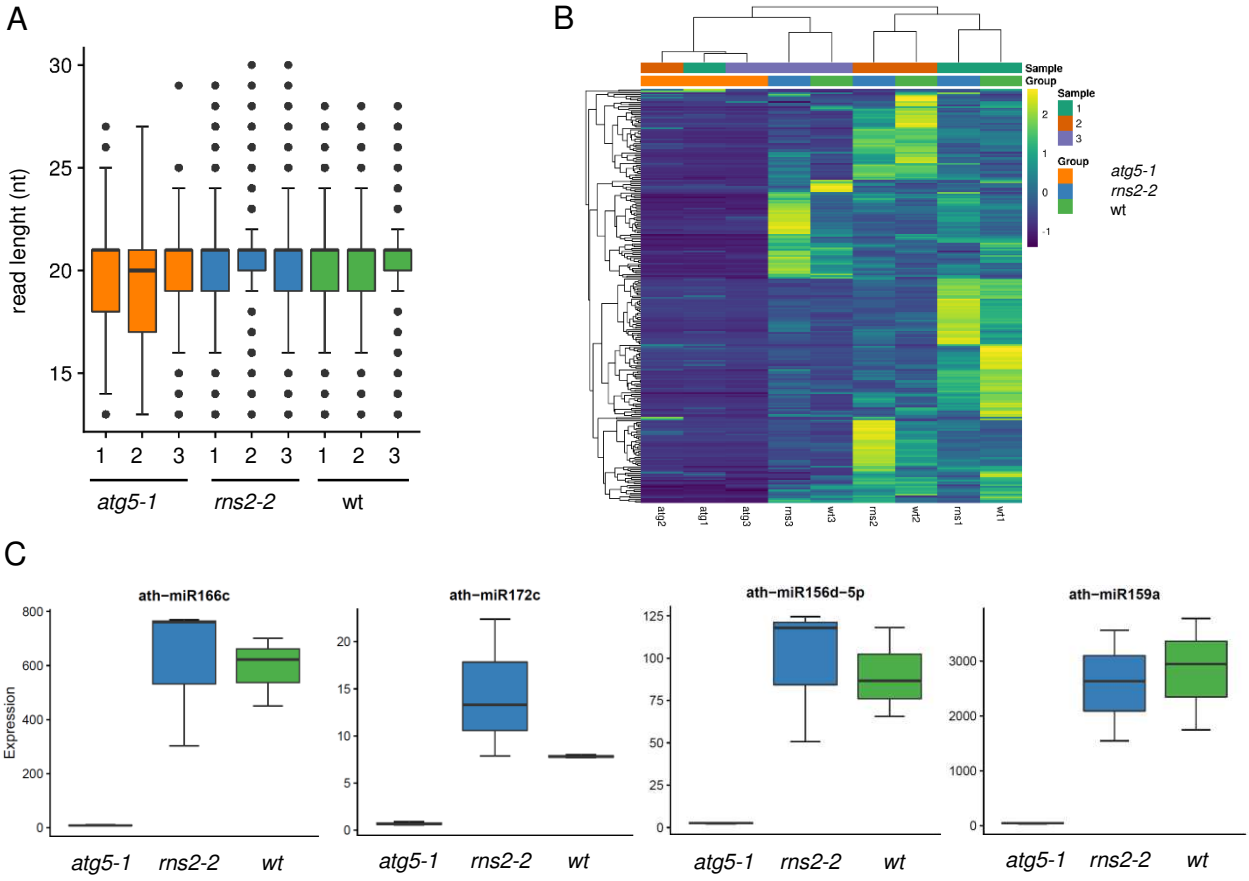

Fig. 5. Analysis of miRNAs found in vacuoles from the three different genotypes. (**A**) Size distributon of miRNAs. A median length of 21nt was observed for most samples. (**B**) Cluster analysis of miRNAs indicated lower amounts in ATG5 plants. (C) typical examples of miRNAs with different frequencies in ATG5 , RNS2 and WT plants.

Supplemental information

Table S3 Characterization of isolated vacuoles. Three replicates of isolated vacuoles from each genotype were prepared and parameters were determined

Isolated vacuoles	WT-1	WT-2	WT-3	ATG5-1	ATG5-2	ATG5-3	RNS2-1	RNS2-2	RNS2-3
α-mann. U ml^{-1} (10^{-3})	1.42	2.06	1.66	2.43	2.24	1.20	2.47	2.48	2.50
GAP-DH U ml^{-1} (10^{-3})	20.82	39.7	42.0	21.6	27.2	30.5	24.6	42.3	40.8
RNA (µg/ml)	39.0	40.9	57.0	38	59.7	44	52.2	81.5	66.1
Protein (µg/ml)	613.0	675	667	686	676	643	676	705	746
Sequencing & data analysis									
Input reads (Million, after trimming)	58	42	8	22	31	12	34	33	14
Average length (bases)	26	25	26	26	24	25	26	26	27
Unique mapped reads (Mio)	11	8	1.4	1.3	1.7	0.6	6	4.6	3.4
Mapped to multiple loci (Mio)	39	28	5.5	19.6	27.3	10.6	23	22	9.3

Table S6: **Primers used in this study**

Gene	s-sequence [5´→3´]	as-sequence [5´→3´]
knockout screening		
LBb1.3	ATTTTGCCGATTTCGGAAC	CTGCTTGCAGTGATTCCTTTC
LB_3	TAGCATCTGAATTTCATAACCAATCTCGATACAC	GAGGCCTGTATATTTCCCCAC
Ef1α_fwd	GAGACCACCAAGTACTACTGCAC	TGGGTTTTCTAACGCATTGAC
Ef1α_rev	GTTGGTCCCTTGTACCAGTCAAG	TCAATGCGTTAGAAAACCCAC
RNS2_fwd	ATGGCGTCACGTTTATGTCTTCTCC	CCACCAAGAGAACTGTAAGCG
RNS2_rev	TCAAAGAGCTTCTCTTTCTGTTGG	TCTTCAGCAAGACACATGTCG
RNS1_RT_fwd	AATCTTGCCTTCTGTCTTCTCTGC	CAAGACCACTCACCACTCCTC
RNS1_RT_rev	GTCACAGTATGATCCTGGCCATTG	AGGGTGACATGGATCAGACAG
RNS2_RT_fwd	CAAGCTGGCTATGTTGCTTCC	GTCGCAAAAAGCTCGTAGTTG
RNS2_RT_rev	GCGTGTATTCCGGCAAACTTACG	TGGTTTTAGCAGCCAAATACG
LP/RP 118507	AGCGAATGGTGGTGCTATATG	TGAGAATCCTTCAGTTCACGG
LP/RP 127028C	CAGCAACGGAGACAGAGAGTC	GGGAGGCACTATGAGGTTAGG
LP/RP 020074C	CCAAAAGCTCAGGTTCTTGTG	TTTTTATTTTGCTTGTTGGCC

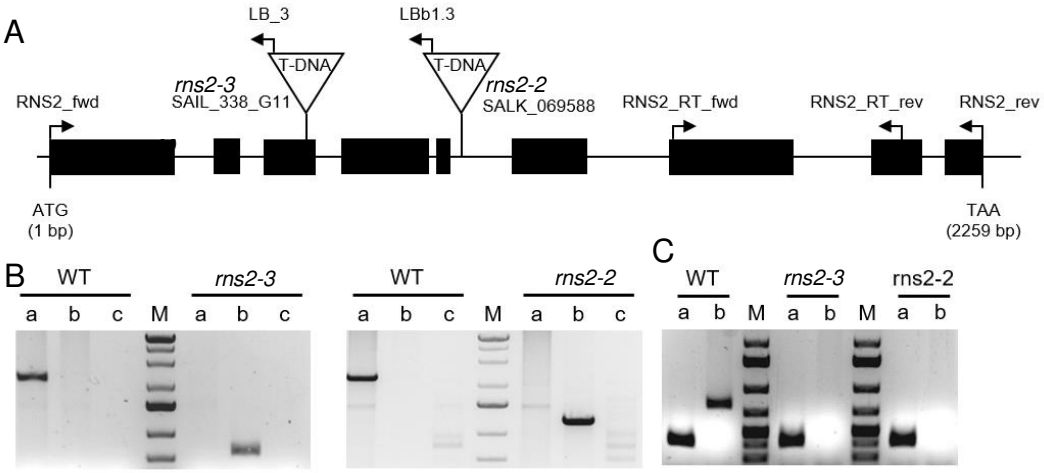

Fig. S1. **Identification of RNS 2-2 and RNS 2-3 T-DNA insertion lines. (A)** Schematic view of the *RNS2* gene with position of T-DNA insertion for the lines SALK_069588 (RNS 2-2) and SAIL_338_G11 (RNS2-3), verified by sequencing of specific PCR products. Exon positions are represented by black rectangles, intron positions and untranslated regions by black lines. Primer binding positions are indicated by arrows. (B) Verification of T-DNA insertion by gDNA based PCR analysis. Primer combinations were chosen for gene specific (a) and T-DNA specific amplification products (b and c) in left and middle panel. (C) Complete loss of *RNS2* gene product and quality of cDNA was checked by gene specific primer combination for *RNS2* (b) and the housekeeping gene EF1α in RT-PCR.

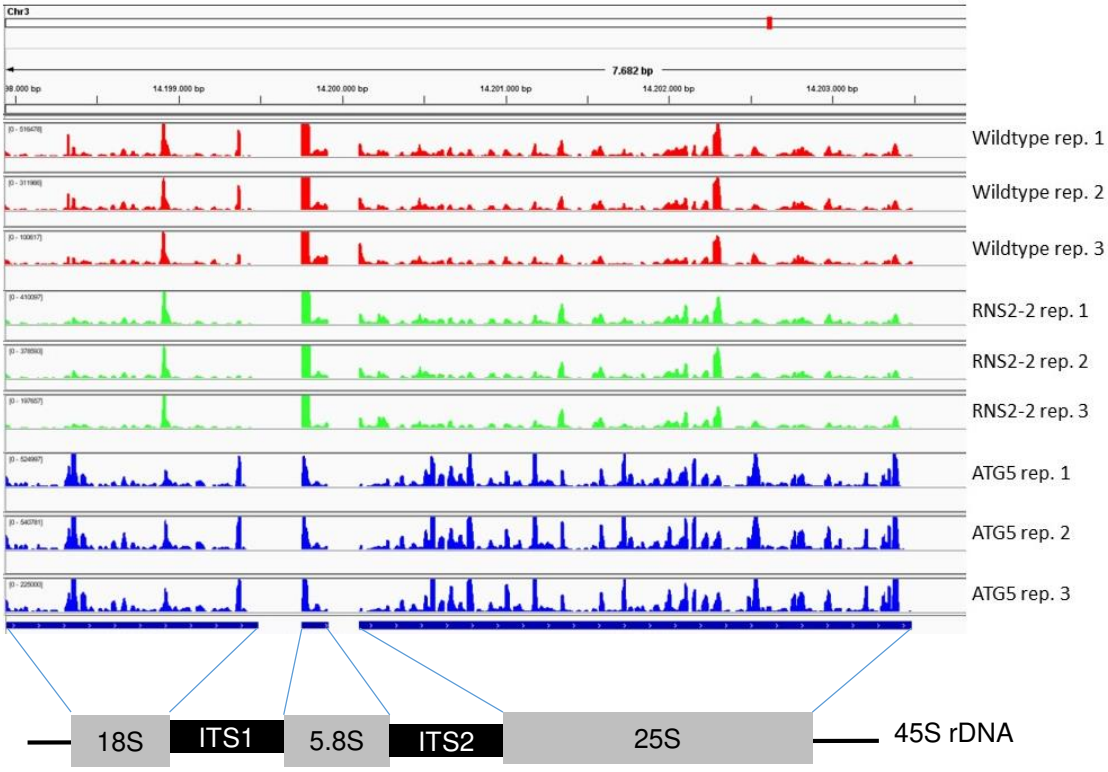

Fig. S2. Accumulated reads on 45S rDNA in wildtype, *rns2-2* and *atg5-1* plants. Illustrated by IGV browser Version 2.4.16 downloaded from the Integrative Genomics Viewer homepage, for 3 biological replicates.